AGU PUBLICATIONS

Geochemistry, Geophysics, Geosystems

TECHNICAL REPORTS: METHODS

10.1002/2016GC006560

Key Points:
- First stereographic use of high speed cameras to reconstruct trajectories of pyroclasts in 3-D
- First-order model allowing a 10° precision for azimuth and dip, and a 20% for velocities
- Applications include Strombolian explosions, bubble bursts in lava lakes and in-flight collisions

Supporting Information:
- Supporting Information S1
- Figure S1
- Movie S1
- Movie S2
- Movie S3

Correspondence to:
D. Gaudin,
damgaudin@gmail.com

Citation:
Gaudin, D., J. Taddeucci, B. F. Houghton, T. R. Orr, D. Andronico, E. Del Bello, U. Kueppers, T. Ricci, and P. Scarlato (2016), 3-D high-speed imaging of volcanic bomb trajectory in basaltic explosive eruptions, *Geochem. Geophys. Geosyst.*, *17*, doi:10.1002/2016GC006560.

Received 26 JUL 2016
Accepted 19 SEP 2016
Accepted article online 00 Month 2016

3-D high-speed imaging of volcanic bomb trajectory in basaltic explosive eruptions

D. Gaudin[1,2], J. Taddeucci[1], B. F. Houghton[3], T. R. Orr[4], D. Andronico[5], E. Del Bello[1], U. Kueppers[2], T. Ricci[1], and P. Scarlato[1]

[1]Istituto Nazionale di Geofisica e Vulcanologia, Sezione di Roma 1, Rome, Italy, [2]Department of Earth and Environmental Sciences, Ludwig-Maximilians-Universität München (LMU), Munich, Germany, [3]University of Hawaii at Manoa, Department of Geology & Geophysics, Honolulu, Hawaii, USA, [4]Hawaiian Volcano Observatory, Hawaii National Park, Hawaii, USA, [5]Istituto Nazionale di Geofisica e Vulcanologia, Sezione di Catania, Osservatorio Etneo, Catania, Italy

Abstract Imaging, in general, and high speed imaging in particular are important emerging tools for the study of explosive volcanic eruptions. However, traditional 2-D video observations cannot measure volcanic ejecta motion toward and away from the camera, strongly hindering our capability to fully determine crucial hazard-related parameters such as explosion directionality and pyroclasts' absolute velocity. In this paper, we use up to three synchronized high-speed cameras to reconstruct pyroclasts trajectories in three dimensions. Classical stereographic techniques are adapted to overcome the difficult observation conditions of active volcanic vents, including the large number of overlapping pyroclasts which may change shape in flight, variable lighting and clouding conditions, and lack of direct access to the target. In particular, we use a laser rangefinder to measure the geometry of the filming setup and manually track pyroclasts on the videos. This method reduces uncertainties to 10° in azimuth and dip angle of the pyroclasts, and down to 20% in the absolute velocity estimation. We demonstrate the potential of this approach by three examples: the development of an explosion at Stromboli, a bubble burst at Halema'uma'u lava lake, and an in-flight collision between two bombs at Stromboli.

1. Introduction

Explosive volcanic activity is characterized by the ejection of fragmented magma (pyroclasts), which are propelled by the release and expansion of pressurized gas. Estimating the ejection velocity of the bombs has a two-fold interest. First, ballistic trajectories and the ranges of deposition of bombs can be estimated from their initial velocity and launch angles [*Tsunematsu et al.*, 2016]. Second, as they are barely decelerated by drag and easy to observe, bombs can be used to infer the burst conditions of gas pockets in basaltic magmas [*Taddeucci et al.*, 2012b; *Gaudin et al.*, 2014b].

Photoballistics studies first used the trace of bombs in long-exposure photographs to determine their initial momentum and launch angle [*Chouet et al.*, 1974]. Average velocity of the particles away or toward the sensor can be estimated with Doppler radars [*Hort et al.*, 2003; *Donnadieu et al.*, 2005]. Recently, high-speed cameras have allowed tracking the displacement of single particles at velocities up to 400 m/s [*Taddeucci et al.*, 2012a; *Vanderkluysen et al.*, 2012; *Gaudin et al.*, 2014a; *Bombrun et al.*, 2015].

However, as for previous methods, only the projection of the trajectory (velocity and angle) of pyroclasts onto a plane perpendicular to the line of sight of the camera is retrieved from high-speed videos. This constraint has severe limitations. First, ejection velocities are always minima, which may lead to an underestimation of important eruptions parameters, e.g., the pressure inside the conduit [*Alatorre-Ibargüengoitia et al.*, 2011; *Del Bello et al.*, 2012; *Taddeucci et al.*, 2012b] or the Mach number in the gas/pyroclasts mixture, crucial for jet noise studies [*Medici et al.*, 2014; *Taddeucci et al.*, 2014]. Second, losing one spatial dimension hinders full understanding of the directionality of the eruption and relating bomb trajectory to final emplacement position.

In this paper, we use multiple, synchronized high-speed videos to obtain a stereoscopic view of the behavior of bomb-sized pyroclasts and reconstruct their full trajectory in the three spatial dimensions and over time. We were faced with several challenges, including: (i) the high velocity and frequent overlapping of the pyroclasts, (ii) highly variable lighting, contrast, and background of the images, (iii) lack of direct access to ground control points close to the target and, (iv) in our case, the use of different models of cameras. These

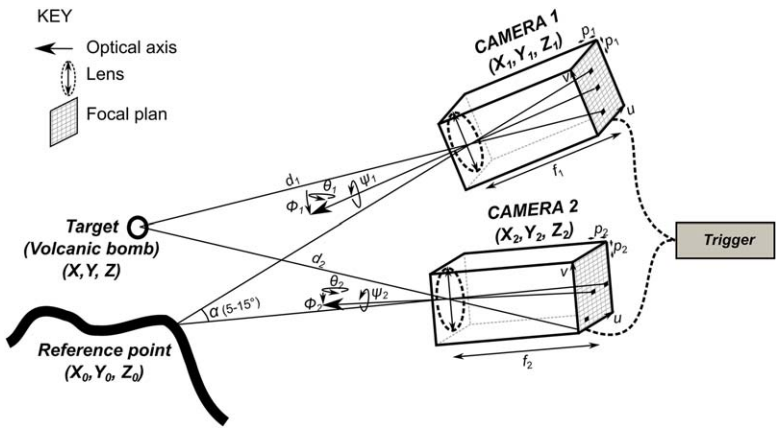

Figure 1. Scheme of the setup and notations used in this report.

limitations prevent the use of automatic correlation algorithms, which are mostly designed for laboratory applications. Instead, we developed a simpler and more robust algorithm, relying on manual tracking of a limited number of representative pyroclasts, and on field measurements of the extrinsic parameters of the cameras (location and orientation). After describing the setup and processing algorithm, we quantify and discuss the uncertainties for the ejection angle, azimuth and velocity of pyroclasts from examples at Stromboli volcano (Italy) and Halema'uma'u lava lake (Hawai'i).

2. Materials and Methods

2.1. Field Setup and Parameter Estimations

Stereographic reconstructions can be achieved from a large variety of set-up, both in terms of resolution, spectral wavelengths and number of cameras. The only requirement is to use at least two cameras, precisely synchronized to avoid the displacement of the targets between equivalent frames of the cameras. For this reason, we used high-speed visible-light cameras recording at least 500 frames per second, connected to the same, external trigger, allowing synchronization within one frame, i.e., 0.002 s. A circular buffer allows the cameras to record a fixed number of frames before and after the trigger frame.

The cameras are placed at locations such that the line of view between the cameras and the target forms an angle of 5–15° (denoted α in Figure 1). These angles have been empirically determined as the best compromise between the precision of the retrieved points (inversely proportional to the sine of this angle) and the ability to recognize from their shape and relative location the same pyroclasts on the different videos.

The geographic position and elevation of a reference camera (X_1, Y_1, Z_1) is estimated by GPS, in our case with a precision of about 10 meters. The relative locations of the other cameras with respect to the reference one are estimated using a laser range finder with a precision of 1 meter and 1 degree, and so is the relative location of a reference, fixed point relatively close to the target (usually some part of the volcanic vent). The azimuth θ and the dip ϕ of the line of sight of each camera are estimated from their geographic position with respect to this reference point, while the roll of the cameras ψ (i.e., the angle of the camera base with the horizontal) is maintained close to zero by using a bubble level (accuracy 4°). All the measurements are repeated three times to minimize and quantify the uncertainties.

2.2. Video Processing and Point Picking

An optional processing step may cancel the shaking due to the wind on each camera by using a correlation technique on a fixed area of the image [*Pan et al.*, 2009]. Finally, the location of individual bombs on each couple or triplet of images, defined by the position of their barycenter, is measured using the MTrackJ plug-in of the ImageJ software [*Abramoff*, 2004; *Meijering et al.*, 2012].

2.3. Stereoscopic Analysis and 3-D Reconstruction

The core of the algorithm consists of computing the 3-D position of the objects from their coordinates (u, v) on the images. For every camera, the collinearity condition associates each point of the image to a line

starting from the camera center, and whose direction (x, y, z) is a function of its coordinates on the focal plane [*Maas et al*., 1993; *Hartley and Zisserman*, 2003]. Considering a geographic coordinate frame where X, Y and Z represent respectively the east, north and altitude coordinates, the orientation of the camera can be described by 3 successive rotations, around Y axis (denoted ψ and sometimes referred as roll), X axis (ϕ, pitch) and Z axis (θ, yaw) [*Hartley and Zisserman*, 2003]. The direction of the line of sight is thus:

$$\begin{pmatrix} x \\ y \\ z \end{pmatrix} = \begin{pmatrix} \cos\theta & -\sin\theta & 0 \\ \sin\theta & \cos\theta & 0 \\ 0 & 0 & 1 \end{pmatrix} \begin{pmatrix} 1 & 0 & 0 \\ 0 & \cos\phi & -\sin\phi \\ 0 & \sin\phi & \cos\phi \end{pmatrix} \begin{pmatrix} \cos\psi & 0 & \sin\psi \\ 0 & 1 & 0 \\ -\sin\psi & 0 & \cos\psi \end{pmatrix} \begin{pmatrix} (u-u_0)p/f \\ 1 \\ (v-v_0)p/f \end{pmatrix} \tag{1}$$

where (u_0, v_0) corresponds to the coordinates of the common reference point measured by the range finder. The focal length f and the size of a physical pixel on the sensor p (pixel pitch) of the camera are provided by the lens and the camera manufacturer.

Denoting (X_c, Y_c, Z_c) the location of the camera, the coordinates (X, Y, Z) of an object are:

$$\begin{pmatrix} X \\ Y \\ Z \end{pmatrix} = \begin{pmatrix} X_c \\ Y_c \\ Z_c \end{pmatrix} + d \begin{pmatrix} x \\ y \\ z \end{pmatrix} \tag{2}$$

where d is the distance from the camera to the object.

With two cameras, equation (2) can be rearranged as:

$$\begin{pmatrix} X_{c,1} \\ Y_{c,1} \\ Z_{c,1} \\ X_{c,2} \\ Y_{c,2} \\ Z_{c,2} \end{pmatrix} = \begin{pmatrix} 1 & 0 & 0 & -x_1 & 0 \\ 0 & 1 & 0 & -y_1 & 0 \\ 0 & 0 & 1 & -z_1 & 0 \\ 1 & 0 & 0 & 0 & -x_2 \\ 0 & 1 & 0 & 0 & -y_2 \\ 0 & 0 & 1 & 0 & -z_2 \end{pmatrix} \begin{pmatrix} X \\ Y \\ Z \\ d_1 \\ d_2 \end{pmatrix} \tag{3}$$

The matrix of unknowns (right term) can be computed by inverting the central matrix using a least squares technique and multiplying it by the coordinate matrix (left term). Note that, if the roll is null, all the equations on Z are quasi-equivalent, so that the problem is not overdetermined. Any additional camera will bring two equations related to $X_{c,n}$ and $Y_{c,n}$, but only one unknown d_n making the problem overdetermined and allowing estimating the uncertainties on the computed parameters.

2.4. Roll Estimation

Roll is the main source of error (see section 3) and, at the same time, the most difficult parameter to measure in the field. Usually, we try to have a horizontal or vertical reference line in the image (e.g., the horizon line or a plumb bob). Otherwise, we developed a method based on the fact that the effect of drag on the slowest and biggest pyroclasts is negligible, so that, in the absence of significant crosswind, their motion is mostly controlled by gravity and their horizontal velocity does not vary significantly.

For instance, if a camera is rolled toward the right, pyroclasts trajectories will appear deviated to the left when going upward, and to the right when going downward, i.e., they experience an apparent acceleration to the right. Consequently, their u coordinates do not linearly correlate with time. Thus, we use a trial and error algorithm to compute the roll for which the average horizontal acceleration of these particles (i.e., in the u direction) vanishes.

2.5. Postprocessing

For a better visualization, the trajectories might be smoothed. If drag forces are negligible with respect to gravity (i.e., under 200 m/s for a 10 cm spherical bomb), trajectories can be also fitted by the equations of ballistics (i.e., linearly on the X and Y coordinates and using a second-order polynomial on the Z coordinate), enabling the backtracking of the particles.

Table 1. Estimation of the Uncertainties for Two Cameras, Located 300 m North of the Target and 30 m Apart (i.e., $\alpha = 5.7°$), With a Focal Length *f* of 300 mm and a Pixel Pitch *p* of 10 μm (i.e., Pixel size of 1 cm)[a]

Parameter	Uncertainty (2σ)	Error in Position			Error on Motion (1 m)			Error on Motion (10 m)		
		X (m)	Y (m)	Z (m)	Vel (%)	Az (°)	Dip (°)	Vel (%)	Az (°)	Dip (°)
Reference point location	5 m	0.07	0.15	0.07	4.1	1.5	0.6	4.2	1.5	0.6
Distance between cameras	2 m	0.01	0.30	0.03	5.2	2.9	1.3	5.4	2.8	1.3
Point pick	2 px	0.01	0.28	0.02	23.2	12.0	5.2	2.4	1.2	0.6
Roll	1°	0.06	0.13	0.00	14.7	7.2	3.4	14.9	7.2	3.3
Total		0.11	0.32	0.02	27.5	14.6	6.3	16.9	8.0	3.7

[a]Uncertainties on locations are estimated by repeating the measurements, while those on point pick and roll are deduced from the videos. The "error in position" column corresponds to the uncertainties on the absolute location for a particle located 500 pixels up and 500 pixels left of the reference point. The "error on motion" columns provides the uncertainties on the absolute velocity, azimuth and dip angle for a particle traveling 1 m to the North, 1 m to the East and 1 m up (respectively 10 m, 10 m and 10 m for the last column).

3. Uncertainties Analysis

In order to assess the reliability and precision of our approach, we quantify the effect of the instrumental and measurement uncertainties on (i) the position of an object, (ii) its absolute velocity and (iii) its azimuth and dip angle. Uncertainties are directly linked to the geometry of the setup and the characteristics of the cameras. In Table 1, we consider a setup with values typical of Stromboli and Halema'uma'u (see section 4). We simulate random errors on different measured parameters and deduce, through the Monte-Carlo technique, how they affect the position, velocity and angle.

Table 1 demonstrates that uncertainties in the location of the reference point and the distance between the two cameras have a relatively small impact on the results. Conversely, the precision of the point picking during manual tracking is important and can be affected by subjective choices of the operator while tracking relatively large bombs. For our setup this parameter can lead to errors up to 12° in azimuth and 23% on the velocity of 1 meter long tracks. However, this error is strongly reduced when considering longer trajectories. Finally, the most crucial source of uncertainties is the roll of the camera. Use of a bubble level allows reaching a precision of 4°, which can be reduced by our correction algorithm (see section 2.4) to about 1°, leading to uncertainties on the azimuth and dip angle of 7° and 3° respectively. The precision of the method could be improved using electronic levels that can reach a precision of 0.1°. Additional tests show that similar uncertainties are retrieved if the target is located at a different altitude from the cameras.

4. Applications

4.1. Time Evolution of a Strombolian Explosion at Stromboli Volcano (Italy)

Strombolian explosions are short-lived (a few to a few tens of seconds) ejection events caused by the burst of overpressurized gas pockets at the upper end of a mafic magma inside the volcanic conduit [e.g., *Blackburn et al.*, 1976]. On 18 May 2014, we monitored the explosive activity of a vent located at the center of the crater terrace of Stromboli. We deployed two high speed cameras on the Pizzo viewpoint, a 914 m high peak overlooking the crater terrace (Figure 2a): an Optronis CR600x2 (1024 × 1280 pixels, 500 frames per second, denoted Cam1) and a Phantom Miro 120, (1216 × 1024 pixels, 1000 frames per second, denoted Cam2) at respective distances of 265 m and 253 m from the vent, forming an angle α of 13.5°. We here focus on a 8 s duration explosion occurred at 11:34:17 GMT that was simultaneously filmed by a thermal camera from the INGV permanent monitoring network (SQT station) located at about 400 m of elevation with a perpendicular point of view (Figure 2a). In total, we tracked 79 bomb trajectories (Figure 2b) and measured 47 reference points along the crater to reconstruct its shape.

The reconstructed 3-D tracks (Figure 3a and supporting video S1) show that, during the first 2 s, pyroclasts are relatively fast and collimated around a mean direction of N150°, and an inclination of 12° from the vertical (Figure 3b). The error bars, computed through a Monte Carlo method, clearly show that this deviation from the vertical is significant, which is also confirmed by the SQT video monitoring system showing a deviation toward the South-East (Figure 3c). Toward the end of the explosion, the absolute velocities of the ejected bombs decrease while their dip angles increase. In addition, the bombs are no longer directed about a specific azimuth but rather distributed in all directions. Most backward extrapolations of the trajectories meet in a 1.1 m ×1.3 m region at a depth of 1.6 m below the vent opening, which may correspond to

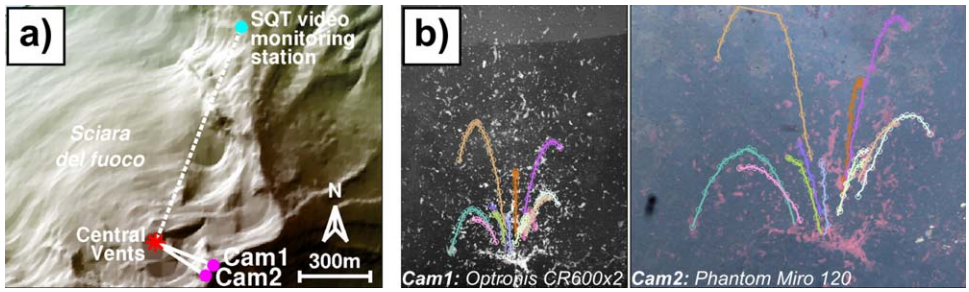

Figure 2. Reconstruction of an explosion in the central vent area at Stromboli (18 May 2014, 11:34:17 GMT). (a) Map showing the location of the two cameras (at Pizzo) with respect to the vents. The SQT video monitoring system is also shown. (b) Coupled still frames (t=4.9s), showing tracked bombs. For clarity, only one fifth of the tracked points are shown.

the depth of the burst [*Dürig et al.*, 2015], which is consistent with previous estimates based on analysis of explosion pulses [*Gaudin et al.*, 2014b].

4.2. Bubble Burst at Halema'uma'u Lava Lake (Hawai'i)

In December 2015, Kīlauea volcano hosted a 210 × 170 m lava lake in the Halema'uma'u crater. This lava lake typically shows spattering activity close to a magma downwelling area ("SE Sink," Figure 4a). This has been interpreted as the burst of single, pressurized gas bubbles [*Patrick et al.*, 2016]. We deployed the *Phantom Miro 120* (details above) together with a *NAC-Memcam HX6* (1920 × 2560 pixels, 500 frames per second) on the rim of Halema'uma'u crater (Figure 4a). The two cameras were placed at 323 and 258 m from the sink, respectively, forming an angle α of 7.4°. During a burst on 9 December 2015, 02:11 GMT (Figure 4b) we tracked 58 individual pyroclasts (supporting figure S1) and measured 80 points on the rim of the overlook crater to reconstruct its shape.

The 3-D reconstruction of the particle trajectories (Figure 4c and supporting video S2) shows that half of the burst is not visible, because it is located under an overhang. Pyroclasts are ejected in two main lobes with

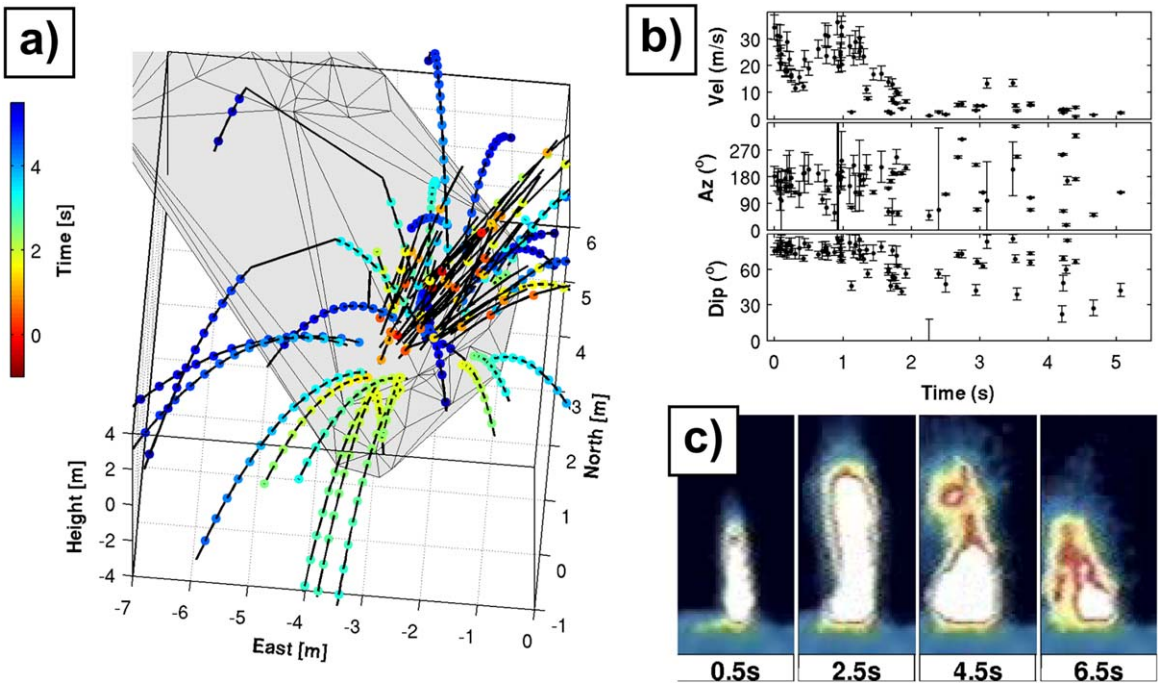

Figure 3. Results of the 3-D reconstruction of the 18 May 2014, 11:34:17 GMT explosion. (a) 3-D smoothed reconstruction of the 79 particle trajectories during the explosion, color-coded for time. The dots represent the location of the successive location of the bombs with a time step of 0.10s. (b) Evolution of the velocity, azimuth and dip angle of the bombs when they exit the vent. Each point represents a single bomb. c) Detail of the explosion seen by the SQT video monitoring system (see location on Figure 2a)).

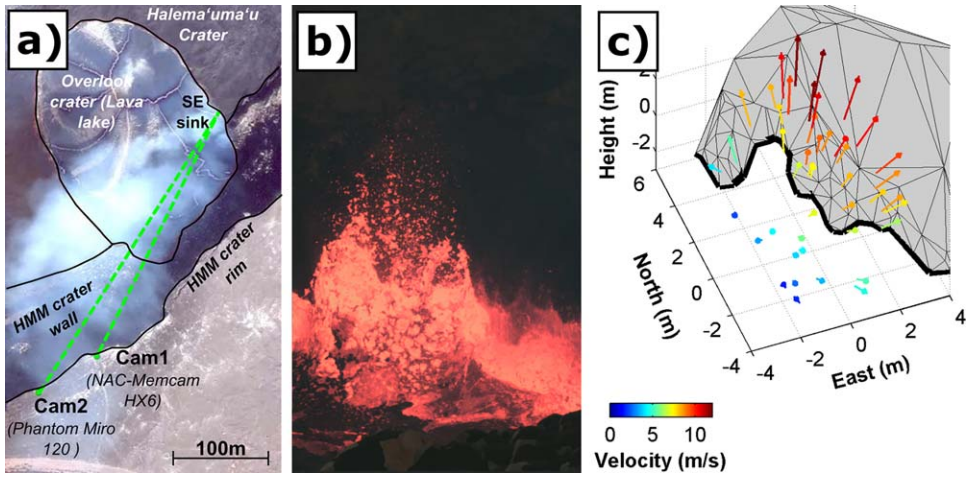

Figure 4. Bubble burst at Halema'uma'u lava lake (9 December 2015, 02:11 GMT). (a) Map of the setup. (b) Detail of a still frame from Cam2 0.5 s after the burst. c) 3-D reconstructions of the particle location and velocity 0.5 s after the burst.

the highest velocities in the left one, suggesting either the occurrence of two district bubbles or a complex burst mechanism due to rheological heterogeneities of the crust of the lava lake.

4.3. In Flight Bomb Collision at Stromboli (Italy)

In-flight collisions can modify the trajectories and velocities of erupted pyroclasts, possibly extending their range [*Vanderkluysen et al.*, 2012]. Using the configuration described in section 4.1, we filmed and reconstructed the trajectories of two bombs colliding, one descending at the time of the collision (Bomb 1, see Figure 5a) and the other one ascending (Bomb 2). During the collision, part of Bomb 1 detaches and adheres to Bomb 2 (see supporting video S3), decreasing the velocity of the latter, while the velocity of Bomb1 does not significantly vary.

The 3-D reconstruction of the trajectories shows that, although the two bombs had initially the same direction (N250°), the descending bomb diverges by approx. 30° due to the collision. This example clearly demonstrates that collisions not only lead to velocity changes but also to the generation of lateral momentum which would be almost impossible to detect with only one camera.

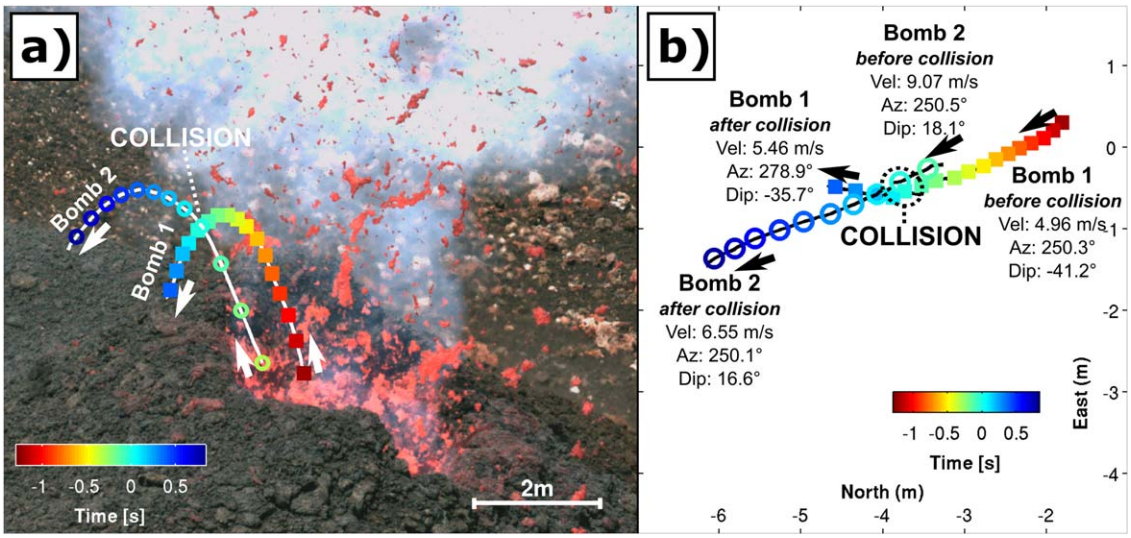

Figure 5. 3-D reconstruction of a bomb collision on 18 May 2014, 10:30:08 GMT, at Stromboli central vent. (a) Still frame from the Phantom Miro 120 camera at the time of the collision, showing the trajectories of the two bombs before and after the collision which occurs at time =0. (b) Map view of the trajectories of the two bombs. Note the change of the angle of the bomb 1, represented by squares. Velocities are computed 0.1s before and after the collision.

5. Discussion and Conclusions

The three examples presented here highlight the potential of our method without ignoring its limitations. Being both easy to set-up in the field and simple to process, the technique allows for a robust 3-D reconstruction of bomb-sized pyroclast trajectories with accuracy of about 5–10° in azimuth and dip, which could be reduced to less than 3° using more accurate distance values and levels. Tests at Stromboli and uncertainties analysis demonstrated that adding a third camera only decreases the errors due to picking by ~30%, with an effect on the final uncertainties limited to less than 5%.

The main limitations of the method are linked to the fact that the tracking is achieved manually. As the technique is time consuming, only a limited number of particles can be tracked. Thus, an automated processing algorithm would be the logical next step. Feature detection and matching algorithms, or even Structure from Motion softwares, could be used for the reconstruction of the background and, with a better location of the cameras, 3-D Lagrangian particle tracking velocimetry could be theoretically used with three or four synchronized cameras [Malik et al., 1993; Ouellette et al., 2005]. Such techniques will face several crucial challenges linked to the high density of particles in the images [Gaudin et al., 2014a] and the synchronization of cameras leading to uncertainties in the position of the particles.

Conversely, our algorithm could be used in numerous contexts, with visible-light but also infrared or UV cameras. In particular, such method enables the accurate calibration of ballistic models for the assessment of volcanic hazard, particularly at highly populated and touristic volcanoes [Tsunematsu et al., 2016]. The observation of multiple bomb trajectories during a Strombolian explosion (section 4.1) allows for computation of the mean direction and the spread angle for the jet, which perhaps reflects the orientation of the shallow conduit [e.g., Dürig et al., 2015] or a differential blocking of the vent. Similarly, the observation of bubble bursting in lava lakes (section 4.2) can provide insights on the burst mechanism, linked to the magma properties. This technique can also be applied to individual bombs, to detect the effects of drag, wind, and in-flight collision (section 4.3) on the deformation, in-flight disintegration and flight path of bombs. By using multiple points on individual bombs, the effect of in-flight deformation and rotation could even be studied. Finally, this technique can be used in other geophysical applications, e.g., rockfalls, man-made explosions or fast ground deformation.

Acknowledgments
The research leading to these results has received funding from the People Programme (Marie Curie Actions) of the European Union's Seventh Framework Programme (FP7/2007-2013) under the project NEMOH, REA grant agreement 289976, NORth, and NSF grants EAR-1145159, and 1427357. The authors thank M. James, M. Jaud and M. Moroni for fruitful discussions, and M. Bombrun, H. Dietterich and an anonymous reviewer who significantly improved the quality of the paper by their constructive reviews. Supporting information are available on the G3 repository. Raw data supporting this paper are available at INGV Roma—Department of Seismology and Tectonophysics, HP-HT lab. Any use of trade, firm, or product names is for descriptive purposes only and does not imply endorsement by the U.S. Government.

References

Abramoff, M. (2004), Image processing with ImageJ, *Biophotonics Int.*, *11*(7), 36–42.
Alatorre-Ibargüengoitia, M. A., B. Scheu, and D. B. Dingwell (2011), Influence of the fragmentation process on the dynamics of Vulcanian eruptions: An experimental approach, *Earth Planet. Sci. Lett.*, *302*(1–2), 51–59, doi:10.1016/j.epsl.2010.11.045.
Blackburn, E. A., L. Wilson, and R. S. J. Sparks (1976), Mechanisms and dynamics of Strombolian activity, *J. Geol. Soc. London*, *132*(4), 429–440, doi:10.1144/gsjgs.132.4.0429.
Bombrun, M., A. Harris, L. Gurioli, J. Battaglia, and V. Barra (2015), Anatomy of a Strombolian eruption: Inferences from particle data recorded with thermal video, *J. Geophys. Res. Solid Earth*, *120*, doi:10.1002/2014JB011556.
Chouet, B., N. Hamisevicz, and T. R. McGetchin (1974), Photoballistics of volcanic jet activity at Stromboli, Italy, *J. Geophys. Res.*, *79*(32), 4961–4976, doi:10.1029/JB079i032p04961.
Del Bello, E., E. W. Llewellin, J. Taddeucci, P. Scarlato, and S. J. Lane (2012), An analytical model for gas overpressure in slug-driven explosions: Insights into Strombolian volcanic eruptions, *J. Geophys. Res.*, *117*, B02206, doi:10.1029/2011JB008747.
Donnadieu, F., G. Dubosclard, R. Cordesses, T. Druitt, C. Hervier, J. Kornprobst, J.-F. Lénat, P. Allard, and M. Coltelli (2005), Remotely monitoring volcanic activity with ground-based Doppler radar, *Eos Trans. AGU*, *86*(21), 201.
Dürig, T., M. T. Gudmundsson, and P. Dellino (2015), Reconstruction of the geometry of volcanic vents by trajectory tracking of fast ejecta—The case of the Eyjafjallajökull 2010 eruption (Iceland), *Earth Planets Space*, *67*(1), 64, doi:10.1186/s40623-015-0243-x.
Gaudin, D., M. Moroni, J. Taddeucci, P. Scarlato, and L. Shindler (2014a), Pyroclast Tracking Velocimetry: A particle tracking velocimetry-based tool for the study of Strombolian explosive eruptions, *J. Geophys. Res. Solid Earth*, *119*, 5369–5383, doi:10.1002/2014JB011095.
Gaudin, D., J. Taddeucci, P. Scarlato, M. Moroni, C. Freda, M. Gaeta, and D. M. Palladino (2014b), Pyroclast Tracking Velocimetry illuminates bomb ejection and explosion dynamics at Stromboli (Italy) and Yasur (Vanuatu) volcanoes, *J. Geophys. Res. Solid Earth*, *119*, 5384–5397, doi:10.1002/2014JB011096.
Hartley, R., and A. Zisserman (2003), *Multiple View Geometry in Computer Vision*, Cambridge Univ. Press, Cambridge, U. K.
Hort, M., R. Seyfried, and M. Vöge (2003), Radar Doppler velocimetry of volcanic eruptions: Theoretical considerations and quantitative documentation of changes in eruptive behaviour at Stromboli volcano, Italy, *Geophys. J. Int.*, *154*(2), 515–532, doi:10.1046/j.1365-246X.2003.01982.x.
Maas, H. G., A. Gruen, and D. Papantoniou (1993), Particle tracking velocimetry in three-dimensional flows, *Exp. Fluids*, *15*(2), 133–146, doi:10.1007/BF00190953.
Malik, N. A., T. Dracos, and D. A. Papantoniou (1993), Particle tracking velocimetry in three-dimensional flows, *Exp. Fluids*, *15*(4–5), 279–294, doi:10.1007/BF00223406.
Medici, E. F., J. S. Allen, and G. P. Waite (2014), Modeling shock waves generated by explosive volcanic eruptions, *Geophys. Res. Lett.*, *41*, 414–421, doi:10.1002/2013GL058340.
Meijering, E., O. Dzyubachyk, and I. Smal (2012), Methods for cell and particle tracking, *Methods Enzymol.*, *504*(9), 183–200.

Ouellette, N. T., H. Xu, and E. Bodenschatz (2005), A quantitative study of three-dimensional Lagrangian particle tracking algorithms, *Exp. Fluids*, *40*(2), 301–313, doi:10.1007/s00348-005-0068-7.

Pan, B., K. Qian, H. Xie, and A. Asundi (2009), Two-dimensional digital image correlation for in-plane displacement and strain measurement: A review, *Meas. Sci. Technol.*, *20*(6), 62001, doi:10.1088/0957-0233/20/6/062001.

Patrick, M. R., T. Orr, A. J. Sutton, E. Lev, W. Thelen, and D. Fee (2016), Shallowly driven fluctuations in lava lake outgassing (gas pistoning), Kīlauea Volcano, *Earth Planet. Sci. Lett.*, *433*, 326–338, doi:10.1016/j.epsl.2015.10.052.

Taddeucci, J., P. Scarlato, A. Capponi, E. Del Bello, C. Cimarelli, D. M. Palladino, and U. Kueppers (2012a), High-speed imaging of Strombolian explosions: The ejection velocity of pyroclasts, *Geophys. Res. Lett.*, *39*, L02301, doi:10.1029/2011GL050404.

Taddeucci, J., M. A. Alatorre-Ibargüengoitia, M. Moroni, L. Tornetta, A. Capponi, P. Scarlato, D. B. Dingwell, and D. De Rita (2012b), Physical parameterization of Strombolian eruptions via experimentally-validated modeling of high-speed observations, *Geophys. Res. Lett.*, *39*, L16306, doi:10.1029/2012GL052772.

Taddeucci, J., J. Sesterhenn, P. Scarlato, K. Stampka, E. Del Bello, J. J. Pena Fernandez, and D. Gaudin (2014), High-speed imaging, acoustic features, and aeroacoustic computations of jet noise from Strombolian (and Vulcanian) explosions, *Geophys. Res. Lett.*, *41*, 3096–3102, doi:10.1002/2014GL059925.

Tsunematsu, K., Y. Ishimine, T. Kaneko, M. Yoshimoto, T. Fujii, and K. Yamaoka (2016), Estimation of ballistic block landing energy during 2014 Mount Ontake eruption, *Earth Planets Space*, *68*, 88, doi:10.1186/s40623-016-0463-8.

Vanderkluysen, L., A. J. L. Harris, K. Kelfoun, C. Bonadonna, and M. Ripepe (2012), Bombs behaving badly: Unexpected trajectories and cooling of volcanic projectiles, *Bull. Volcanol.*, *74*(8), 1849–1858, doi:10.1007/s00445-012-0635-8.